# Transport properties of $Bi_{1-x}Sb_x$ alloy nanowires synthesized by pressure injection

Yu-Ming Lin,[a] S. B. Cronin,[b] O. Rabin,[c] Jackie Y. Ying,[d] and M. S. Dresselhaus[a),b),e)]
*Massachusetts Institute of Technology, Cambridge, Massachusetts 02139-4307*

(Received 30 January 2001; accepted for publication 25 May 2001)

Various transport measurements are performed to assess the alloying and size effects in sub-100 nm $Bi_{1-x}Sb_x$ ($0 \leqslant x \leqslant 0.15$) nanowires. Temperature-dependent resistance measurements exhibit non-monotonic trends as $x$ increases, and a theoretical model is presented to explain the features which are related to the unusual band structure of $Bi_{1-x}Sb_x$ systems. Magnetoresistance measurements of these $Bi_{1-x}Sb_x$ nanowires show interesting size-dependent behaviors similar to those in Bi nanowires. © *2001 American Institute of Physics.* [DOI: 10.1063/1.1385800]

Nanostructured materials have received much attention recently because they are expected to exhibit very different properties from their bulk counterparts due to quantum confinement effects. The ability to tailor materials properties by exploiting quantum confinement effects[1] not only provides a promising approach for device optimization, but also creates possibilities for fundamental studies and nanotechnological applications.[2]

Bismuth (Bi) is a very attractive material for transport studies in low-dimensional systems. The electrons in Bi are distributed in three highly anisotropic carrier pockets at the $L$ points of the Brillouin zone, and the holes are contained in one pocket at the $T$ point.[3,4] Quantum confinement effects can be readily observed in Bi at a larger size scale ($\sim$50 nm) than for most other metals or semiconductors.[5] $Bi_{1-x}Sb_x$ alloys form substitutional solid solutions, and the band structure of these alloys changes gradually from that of Bi to that of Sb as $x$ increases.[6,7] Thus, $Bi_{1-x}Sb_x$ nanowires constitute a unique 1D system in which the band structure and other related properties can be tailored by combining quantum confinement effects with Sb alloying effects. With the addition of Sb, it is possible to increase the critical diameter for the semimetal–semiconductor transition from $\sim 50$ nm to $\geqslant 100$ nm in a controlled manner and to study this transition behavior systematically.[8,9]

The transport properties of $Bi_{1-x}Sb_x$ alloys in bulk form[10,11] and in thin films[12,13] have been studied extensively because of their promising thermoelectric efficiency at low temperatures. In $Bi_{1-x}Sb_x$ alloys, the six $H$-point hole pockets have to be considered for transport phenomena in addition to carriers in the $L$- and $H$-point pockets, especially for $x \geqslant 0.10$. By manipulating carriers in these various pockets, many ideas that are central to the carrier pocket engineering concept[14] can be applied to the $Bi_{1-x}Sb_x$ nanowire system. It has thus been recently predicted that the thermoelectric efficiency of $Bi_{1-x}Sb_x$ nanowires can be significantly enhanced relative to Bi nanowires,[9] especially for $p$-type wires. We here report experimental temperature and magnetic field dependent transport studies of $Bi_{1-x}Sb_x$ nanowires for $0 \leqslant x \leqslant 0.15$ and compare them with theoretical calculations to better understand their transport properties and to test the validity of the model calculations regarding alloying and size effects.

$Bi_{1-x}Sb_x$ nanowire arrays were synthesized by pressure injecting the molten alloys into anodic alumina thin films,[15,16] following similar procedures described previously.[17–19] $Bi_{1-x}Sb_x$ nanowires of two different diameters (40 and 65 nm) with $x=0$, 0.05, 0.10, and 0.15 were prepared. X-ray diffraction experiments show that the nanowire crystal structure is not affected by alloying with Sb ($\leqslant$15 at. %), and the nanowires have a preferred crystal orientation with the (012) lattice plane perpendicular to the wire axes, consistent with previous observations on pure Bi nanowires.[17]

Figure 1 shows the measured $R(T)/R(270\ \mathrm{K})$ of 40-nm $Bi_{1-x}Sb_x$ nanowires with various $x$ values for $2 \leqslant T \leqslant 300$ K. The resistance of these nanowires increases as $T$ decreases from 300 to 2 K, and saturates at low $T$, which is due to an impurity band resulting from uncontrolled impurity atoms. Because of the low intrinsic carrier density $n_{\mathrm{int}}$ in $Bi_{1-x}Sb_x$ alloys ($\sim 10^{17}$ cm$^{-3}$ at 80 K),[6] even with the highest purity (99.9999%) material, the impurity concentrations ($\sim 10^{16}$ cm$^{-3}$) are still comparable to $n_{\mathrm{int}}$. Since Bi and $Bi_{1-x}Sb_x$ have very small electron effective masses and a high dielectric constant ($\sim$100),[20] the binding energies of the electrons to impurity atoms are very small ($\sim 1.4 \times 10^{-5}$ eV).[13] Therefore, essentially all impurity atoms are ionized, and the extrinsic carriers contribute significantly to the transport phenomena, even at low $T$.

In Fig. 1, although the 40-nm $Bi_{1-x}Sb_x$ nanowires ($x \leqslant 0.15$) all exhibit a qualitatively similar $T$-dependent resistance, the trends are different in detail as a result of Sb alloying. The normalized low-$T$ resistance $R(4\ \mathrm{K})/R(270\ \mathrm{K})$ shows a non-monotonic behavior as $x$ increases, due to competing interactions, resulting from variations in the band structure and carrier mobilities, as explained by the following theoretical modeling. Since the band structure parameters of $Bi_{1-x}Sb_x$ alloys are highly $T$ dependent for $T \geqslant 80$ K,[21] and most of them are well known at lower temperatures ($T \leqslant 100$ K), it is proper to compare the experiments with

[a)]Department of Electrical Engineering and Computer Science.
[b)]Department of Physics.
[c)]Department of Chemistry.
[d)]Department of Chemical Engineering.
[e)]Electronic mail: millie@mgm.mit.edu

 

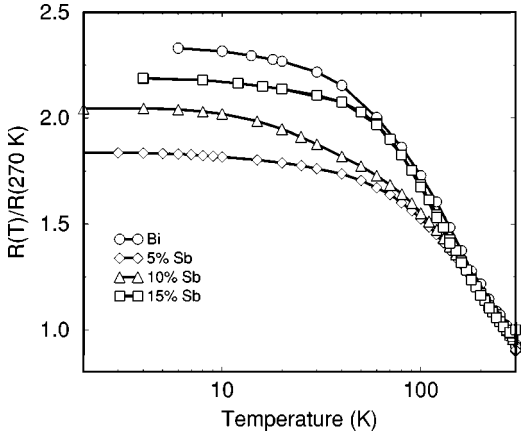


FIG. 1. Measured temperature dependence of the normalized resistance $R(\mathrm{T})/R(270\ \mathrm{K})$ 40-nm $Bi_{1-x}Sb_x$ nanowires for $0 \leqslant x \leqslant 0.15$.

theory for $T \leqslant 100$ K. The electrical conductivity of a system with multiple carriers is expressed as

$$\sigma = \sum_i en_i\mu_i = en_{\mathrm{tot}} \sum_i \gamma_i \mu_i , \tag{1}$$

where $n_i$ and $\mu_i$ are the carrier density and mobility for each type of carrier, respectively, $n_{\mathrm{tot}} = \Sigma_i n_i$ is the total carrier concentration, and $\gamma_i \equiv n_i / n_{\mathrm{tot}}$ are their relative populations.

In Fig. 1, the resistance ratios $R(10\ \mathrm{K})/R(100\ \mathrm{K})$ of $Bi_{1-x}Sb_x$ nanowire arrays are 1.34, 1.19, 1.30, and 1.29 for $x = 0$, 0.05, 0.10, and 0.15, respectively. To understand the transport behavior of $Bi_{1-x}Sb_x$ nanowires as a function of $x$, we examine both the change of $n_{\mathrm{tot}}$ and $\gamma_i$ between 10 and 100 K. The carrier concentrations of $Bi_{1-x}Sb_x$ nanowires are calculated for wires oriented along the trigonal direction, based on the band structure parameters of bulk $Bi_{1-x}Sb_x$ alloys,[7,9] using a numerical method for cylindrical quantum wire calculations.[8] Assuming a modest $n$-type impurity concentration of $10^{16}$ $\mathrm{cm}^{-3}$, the total carrier concentration ratio $n(100\ \mathrm{K})/n(10\ \mathrm{K})$ of 40-nm $Bi_{1-x}Sb_x$ nanowires is calculated as a function of $x$ [see Fig. 2(a)]. Here $n(100\ \mathrm{K})/n(10\ \mathrm{K})$ decreases rapidly as $x$ increases from 0 to 0.10, and becomes relatively flat for $x \geqslant 0.10$. Figure 2(b) shows the difference in the relative carrier population $\Delta\gamma_i = \gamma_i(10\ \mathrm{K}) - \gamma_i(100\ \mathrm{K})$ calculated for 40-nm $Bi_{1-x}Sb_x$ nanowires between 10 and 100 K for the $L$-, $T$-, and $H$-point carriers, and $\gamma_L$ includes contributions from the light-mass $L$-point electrons and holes, which have mirror-like dispersion relations. Since the $L$-point carriers have a much higher mobility than the $T$- and $H$-point holes, the average mobility $\mu_{\mathrm{avg}} = \Sigma_i \gamma_i \mu_i$ is usually dominated by $\gamma_L$. Qualitatively, a larger value of $\Delta\gamma_L$ implies a larger increase in $\mu_{\mathrm{avg}}$ as $T$ decreases, which tends to lower the value of $R(10\ \mathrm{K})/R(100\ \mathrm{K})$. In Fig. 2(b), $\Delta\gamma_L$, $\Delta\gamma_T$, and $\Delta\gamma_H$ are relatively constant for $x \leqslant 0.05$, because the $L$-point electrons and the $T$-point holes are still the two dominant carrier types. As $x$ increases ($0.05 \leqslant x \leqslant 0.12$), the valence band edge energy at the $T$ point moves down, eventually reaching below the $L$-point holes, and the alloy behaves more like a direct-gap semiconductor, with more holes being distributed to the $L$-point pockets. Therefore, $\Delta\gamma_L$ drops rapidly as $x$ increases from 0.05 to 0.12. The $H$-point holes, which gradually become the dominant hole carriers for $x \geqslant 0.12$,

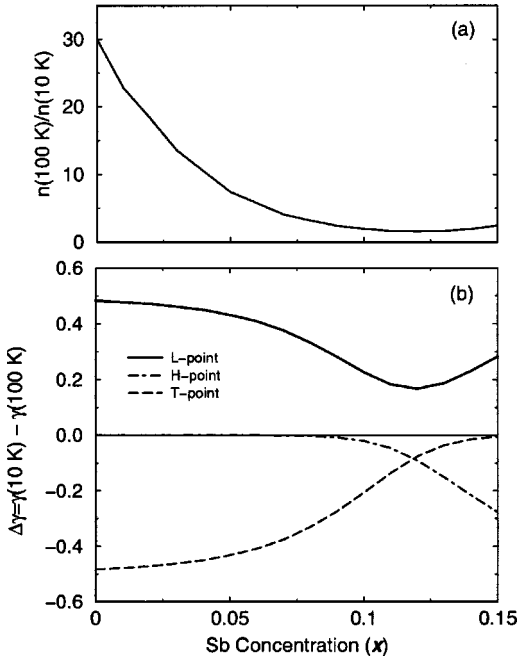


FIG. 2. (a) Calculated ratios of $n(100\ \mathrm{K})/n(10\ \mathrm{K})$ for 40-nm $Bi_{1-x}Sb_x$ alloy nanowires as a function of $x$. (b) Calculated difference of the relative populations $\Delta\gamma_i = \gamma_i(10\ \mathrm{K}) - \gamma_i(100\ \mathrm{K})$ for $L$-, $T$-, and $H$-point carriers in 40-nm $Bi_{1-x}Sb_x$ nanowires.

cause $\Delta\gamma_L$ and $|\Delta\gamma_H|$ to rise with increasing $x$. The measured $R(10\ \mathrm{K})/R(100\ \mathrm{K})$ of 40-nm $Bi_{1-x}Sb_x$ nanowires then can be understood based on the calculations shown in Figs. 2(a) and 2(b). For $x \leqslant 0.05$, since $\Delta\gamma_L$ is almost constant, $R(10\ \mathrm{K})/R(100\ \mathrm{K})$ is mainly determined by the variation of $n(100\ \mathrm{K})/n(10\ \mathrm{K})$, both of which decrease as $x$ increases. For $x \geqslant 0.5$, $n(100\ \mathrm{K})/n(10\ \mathrm{K})$ is less sensitive to $x$, and the variation of $\Delta\gamma_L$ becomes the dominant factor. The decrease of $\Delta\gamma_L$ from 0.43 to $\sim$0.2 is mainly responsible for the increase of $R(10\ \mathrm{K})/R(100\ \mathrm{K})$ as $x$ increases from 0.05 to 0.10. Finally, since the values of $n(100\ \mathrm{K})/n(10\ \mathrm{K})$ are approximately equal for $x = 0.10$ and 0.15 while $\Delta\gamma_L$ is slightly higher for $x = 0.15$, we expect a lower value of $R(10\ \mathrm{K})/R(100\ \mathrm{K})$ for $x = 0.15$ than for $x = 0.10$, consistent with our experimental results.

Figure 3(a) shows the longitudinal magnetoresistance (MR) of 40-nm $Bi_{1-x}Sb_x$ nanowires ($x = 0.15$) as a function of magnetic field $B$ at different temperatures. Other 40-nm-nanowire samples with smaller $x$ values were also measured, and they exhibited MR($B$) trends similar to Fig. 3(a). For $T \geqslant 4$ K, the MR at low $B$ can be described by a parabolic relation $\mathrm{MR} \equiv [R(B) - R(B=0)]/R(B) = A_0 B^2$, where $A_0$ is the magnetoresistance coefficient. In Fig. 3(a), $A_0$ increases with decreasing $T$, consistent with a decrease in electron–photon scattering as $T$ decreases. For all samples, as $T$ decreases below 4 K, the MR exhibits a behavior rather distinct from that at higher $T$, as indicated by the arrow in Fig. 3(a). This special feature is seen in the first derivative of each of the MR curves [see inset of Fig. 3(a)]. This feature, observed previously in Bi nanowires,[22] is attributed to transitional 1D–3D localization effects associated with having the magnetic length $L_H = (\hbar/eB)^{1/2}$ equal the wire diameter $d_w$, and having a long phase breaking length ($L_\phi \geqslant d_w$). The peak of the $dR/dB$ curve at 2 K in Fig. 3(a) occurs at $B_p \sim 0.3$ T,

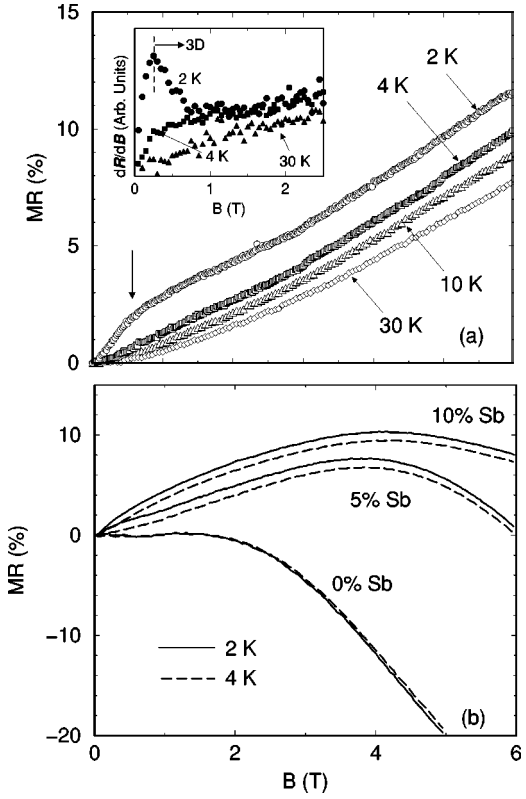


FIG. 3. (a) Longitudinal magnetoresistance of 40-nm $Bi_{1-x}Sb_x$ ($x=0.15$) nanowires as a function of magnetic field at different temperatures. The inset shows the first derivative ($dR/dB$) of the MR. (b) Longitudinal MR as a function of $B$ for larger-diameter ($d_w=65$ nm) $Bi_{1-x}Sb_x$ nanowire arrays. The maximum in MR is attributed to boundary scattering effects.

corresponding to $L_H \sim 47$ nm, very close to the nominal $d_w$ of 40 nm. It is interesting that $B_p$ is independent of $x$, suggesting that the 1D–3D localization phenomenon is a universal effect in nanowires at low $T$.

Figure 3(b) shows the measured MR as a function of $B$ for $Bi_{1-x}Sb_x$ nanowires of a larger diameter ($d_w=65$ nm). The 1D–3D transitional localization effect, although weaker than in the 40 nm diameter wires, is observed at a lower $B$, consistent with theoretical expectations.[22] Other interesting features are the non-monotonic MR($B$) behavior and the maximum observed in the longitudinal MR (e.g., at $B \sim 4$ T for $x \geqslant 0.05$), which is attributed to wire-boundary scattering effects.[23] In the presence of a magnetic field, the trajectory of the mobile carriers is deflected, increasing the probability of wire-boundary scattering at low $B$. However, as $B$ increases beyond a critical field $B_M$, such that the cyclotron orbits of the carriers lie within the wires, the probability of wire-boundary scattering will be reduced, resulting in a decrease in the MR. In Fig. 3(b), the field $B_M$ for the maximum MR increases with increasing $x$ due to the relative strengths of wire-boundary and impurity scattering for electrons. Since neutral impurity scattering makes a greater contribution to the transport in the alloy wires than in pure Bi nanowires, a greater field is needed to reduce the wire-boundary scattering and observe a decreased MR. Our results show that the addition of Sb does not destroy the ballistic transport in pure Bi nanowires,[23] and also confirms long carrier mean free paths and a high crystalline quality in our $Bi_{1-x}Sb_x$ nanowires.

In summary, we present transport measurements of $Bi_{1-x}Sb_x$ nanowire arrays for $0 \leqslant x \leqslant 0.15$. The 1D–3D localization behavior and the wire-boundary scattering effects are observed in the longitudinal MR. Most importantly, the normalized $T$-dependent resistance of 40-nm $Bi_{1-x}Sb_x$ nanowires $[R(T)/R(270\ \mathrm{K})]$ exhibits an unusual *non-monotonic* variation as a function of $x$, which is explained by our model calculations, confirming the validity of our theoretical models and giving vital information on the unusual band structure of $Bi_{1-x}Sb_x$ nanowires, validating the use of carrier pocket engineering[14] to design devices based on this system.

The authors thank Drs. G. Dresselhaus, G. Chen, and J. Heremans for valuable discussions. Support from MURI Subcontract 0205-G-BB853, NSF Grant DMR-98-04734, and U.S. Navy Contract N00167-98-K-0024 is gratefully acknowledged.

[1] L. D. Hicks and M. S. Dresselhaus, Phys. Rev. B **47**, 16631 (1993).
[2] D. Routkevitch, A. A. Tager, J. Haruyama, D. Almawlawi, M. Moskovits, and J. M. Xu, IEEE Trans. Electron Devices **43**, 1646 (1996).
[3] R. T. Isaacson and G. A. Williams, Phys. Rev. **185**, 682 (1969).
[4] J. Heremans and O. P. Hansen, J. Phys. C **12**, 3483 (1979).
[5] J. Heremans, C. M. Thrush, Y. M. Lin, S. Cronin, Z. Zhang, M. S. Dresselhaus, and J. F. Mansfield, Phys. Rev. B **61**, 2921 (2000).
[6] H. J. Goldsmid, Phys. Status Solidi A **1**, 7 (1970).
[7] B. Lenoir, A. Dauscher, X. Devaux, Yu. I. Ravich, R. Martin-Lopez, H. Scherrer, and S. Scherrer, in *Proceedings of the 15th International Conference on Thermoelectrics*, *Pasadena, CA* (IEEE, New York, 1996), p. 1.
[8] Y. M. Lin, X. Sun, and M. S. Dresselhaus, Phys. Rev. B **62**, 4610 (2000).
[9] O. Rabin, Y. M. Lin, and M. S. Dresselhaus, Appl. Phys. Lett. **79**, 81 (2001).
[10] B. Lenoir, M. O. Selme, A. Demouge, H. Scherrer, Yu. V. Ivanov, and Yu. I. Ravich, Phys. Rev. B **57**, 11242 (1998).
[11] W. M. Yim and A. Amith, Solid-State Electron. **15**, 1141 (1972).
[12] D. T. Morelli, D. L. Partin, and J. Heremans, Semicond. Sci. Technol. **5**, S257 (1990).
[13] S. Cho, A. DiVenere, G. K. Wong, and J. B. Ketterson, Phys. Rev. B **59**, 10691 (1999).
[14] T. Koga, X. Sun, S. B. Cronin, and M. S. Dresselhaus, Appl. Phys. Lett. **73**, 2950 (1998).
[15] A. P. Li, F. Müller, A. Birner, K. Neilsch, and U. Gösele, J. Appl. Phys. **84**, 6023 (1998).
[16] H. Masuda, H. Yamada, M. Satoh, H. Asoh, M. Nakao, and T. Tamamura, Appl. Phys. Lett. **71**, 2770 (1997).
[17] Z. Zhang, J. Y. Ying, and M. S. Dresselhaus, J. Mater. Res. **13**, 1745 (1998).
[18] Y.-M. Lin, S. B. Cronin, O. Rabin, J. Heremans, M. S. Dresselhaus, and J. Y. Ying, Mater. Res. Soc. Symp. Proc. **635** (in press).
[19] Y.-M. Lin, S. B. Cronin, J. Y. Ying, M. S. Dresselhaus, and J. P. Heremans, Appl. Phys. Lett. **76**, 3944 (2000).
[20] W. S. Boyle and A. D. Brailsford, Phys. Rev. **120**, 1943 (1960).
[21] M. P. Vecchi and M. S. Dresselhaus, Phys. Rev. B **10**, 771 (1974).
[22] J. Heremans, C. M. Thrush, Z. Zhang, X. Sun, M. S. Dresselhaus, J. Y. Ying, and D. T. Morelli, Phys. Rev. B **58**, R10091 (1998).
[23] Z. Zhang, X. Sun, M. S. Dresselhaus, J. Y. Ying, and J. Heremans, Appl. Phys. Lett. **73**, 1589 (1998).